International Journal of Microwave and Wireless Technologies

cambridge.org/mrf

Beamforming generation via conditional variational autoencoder and adversarial learning

Yuhao Zhang[1], Hongjun Chu[2], Wenzhi Li[2], Zhaohui Song[2] and Xingyu Zhou[1]

[1]School of Communication Engineering, Hangzhou Dianzi University, Hangzhou, China and [2]Space Information Research Institute, Hangzhou Dianzi University, Hangzhou, China

Research Paper

Cite this article: Zhang Y, Chu H, Li W, Song Z, Zhou X (2026) Beamforming generation via conditional variational autoencoder and adversarial learning. *International Journal of Microwave and Wireless Technologies*, 1–8. https://doi.org/10.1017/S1759078726103882

Received: 3 September 2025 UTC
Revised: 30 August 2026 UTC
Accepted: 17 September 2026 UTC

Keywords:
Antenna Design; EM Field Theory; Modelling and Measurements

Corresponding author: Hongjun Chu; Email: chj_hd@hdu.edu.cn

Abstract

To address the limitations of current array antenna beamforming methods in terms of prediction accuracy and generalization capability, this paper proposes an efficient deep learning-based beamforming approach. The method first employs high-precision numerical computations in conjunction with an improved genetic algorithm to optimize the design and generate datasets that closely resemble practical scenarios, thereby providing a solid foundation for neural network training. On this basis, a generative model architecture combining a conditional variational autoencoder and a generative adversarial network is designed to enable accurate and efficient beamforming prediction. Experimental results demonstrate that the proposed method achieves superior performance in planar array scenarios, with improved beam control accuracy compared to typical deep learning models, while significantly reducing computational complexity relative to conventional optimization algorithms.

Introduction

With the increasing demand for efficient resource utilization and high-precision target perception in intelligent communication and radar systems, beamforming technology, as a core technique in array antenna signal processing, plays a crucial role in tasks such as directional radiation [1], interference suppression [2], and multi-target tracking [3]. Existing beamforming methods primarily rely on numerical computations and optimization algorithms [4, 5], in which iterative solutions are employed to control beam patterns [6]. Although these methods can partially meet design requirements, they still suffer from long response times and low convergence efficiency in complex constrained scenarios [7], such as large-scale phased arrays with strict sidelobe level constraints and limited dynamic range of phase shifters. To improve optimization efficiency, some studies have proposed genetic algorithms (GAs) with adaptive switching of multiple mutation parameters to accelerate array pattern synthesis [8]. However, under large-scale planar array settings, these methods still face high computational complexity and long solving times, making it difficult to meet real-time requirements.

In addition, due to the complex coupling effects among array elements, existing approaches also encounter limitations in beamforming accuracy. For instance, some studies have utilized full-wave simulations to extract element radiation data in order to enhance precision [9]. Nevertheless, these methods fail to adequately account for the dynamic influence of varying radiation directions on element coupling, leading to discrepancies between theoretical and practical beam performance.

In recent years, deep learning techniques have demonstrated outstanding feature modeling capabilities and generalization performance in the fields of communications and sensing, gradually emerging as a promising approach to address beamforming problems [10]. Some studies have attempted to replace traditional optimization algorithms with neural networks, aiming to reduce computation time and enhance system robustness [11]. For example, [12] proposed a radial basis function neural network (RBFNN)-based beamforming method for rapid beam design, effectively reducing computational complexity. However, its performance is constrained by the shallow network architecture and limited number of neurons, resulting in weak generalization. To overcome these drawbacks, another study developed a hybrid beamforming scheme based on convolutional neural networks (CNNs) and multilayer perceptrons (MLPs) [13], which improved the ability to capture complex features and achieved certain success in real-time beamforming. Nevertheless, most of these methods have been designed for linear arrays, and they still suffer from insufficient accuracy and poor adaptability to unseen samples when applied to complex planar array scenarios.

© The Author(s), 2026. Published by Cambridge University Press in association with The European Microwave Association.

Downloaded from https://www.cambridge.org/core. UNIVERSIDAD AUTONOMA METROPOLITANA, on 11 Nov 2026 at 21:43:48, subject to the Cambridge Core terms of use, available at https://www.cambridge.org/core/terms. https://doi.org/10.1017/S1759078726103882

In this paper, we propose a beamforming model that integrates a conditional variational autoencoder and a generative adversarial network (CVAE-GAN) to achieve high-precision modeling and prediction of phase distributions in two-dimensional (2D) planar arrays. Specifically, representative training datasets are first generated using an improved genetic algorithm (IGA), covering multiple steering angles and typical beam structures. Then, a CVAE-GAN architecture is constructed, in which the encoder extracts joint features from input phase maps and conditional information, the generator reconstructs the predicted phase distributions, and the discriminator distinguishes between predicted and real samples, thereby improving generation quality. Finally, the model's reconstruction and prediction accuracy are validated using multi-angle test sets.

Experimental results show that the proposed CVAE-GAN model achieves a full-angle error index of 1.65 (measured by $\log(1 + |\text{error}|)$, with the reference standard being beam patterns generated from ground-truth phases) in the synthesized radiation patterns at specified steering angles. This represents a significant reduction compared with the RBFNN model (6.45), with an average error reduction of approximately 4.80, and also outperforms the MLP model (3.99). These results show that the proposed CVAE-GAN has better performance compared with other models, providing a valuable reference for efficient beam design in dynamic scenarios involving planar arrays. Importantly, the proposed framework is developed with a focus on scalability and generalization: while validated on a compact 4×4 array, the CVAE-GAN architecture is inherently tailored for large-scale and multi-constraint scenarios, where conventional iterative solvers suffer from prohibitive computational costs.

Problem formulation

Consider an $M \times N$ uniform planar array (UPA) with inter-element spacing $d = \lambda/2$. For an incident signal with elevation angle θ and azimuth angle ϕ, the direction-cosine variables are defined as $u = \sin\theta \sin\phi$, $v = \sin\theta \cos\phi$. The steering vector is given by

$$\mathbf{a}(u,v) = \left[e^{j\psi_1(u,v)}, \quad e^{j\psi_2(u,v)}, \quad \ldots, \quad e^{j\psi_{N^2}(u,v)}\right]^H \tag{1}$$

with phase term

$$\psi_{i,j}(u,v) = k(i-1)du + k(j-1)dv, \quad i,j = 1,\ldots,N \tag{2}$$

where $k = \frac{2\pi}{\lambda}$ is the wavenumber. The array factor is expressed as

$$\mathrm{AF}(u,v) = \mathbf{w}^H \mathbf{a}(u,v) \tag{3}$$

and the overall array pattern, using the pattern multiplication theorem, is

$$f(u,v) = f_e(u,v)\, \mathbf{w}^H \mathbf{a}(u,v) \tag{4}$$

where $f_e(\theta,\phi)$ denotes the element pattern. The beamforming design aims to achieve unit gain in the main-lobe direction (u_d, v_d), while suppressing radiation in the sidelobe (u_s, v_s) and nulling regions (u_n, v_n). The optimization problem can be formulated as

$$\begin{aligned} &\text{find} \quad \mathbf{w} \\ &\text{s.t.} \quad |f(u_d,v_d)|^2 = 1, \\ &\qquad |f(u_s,v_s)|^2 < \rho, \\ &\qquad |f(u_n,v_n)|^2 < \eta, \end{aligned} \tag{5}$$

where ρ and η denote the maximum allowable sidelobe and interference levels, respectively.

CVAE-GAN neural network architecture

Network structure

To address the beamforming prediction task of phased array antennas, this paper proposes a generative model architecture based on the integration of a CVAE-GAN. The proposed model combines the conditional generation capability of CVAE with the high-quality generation ability of GAN. CNNs are introduced into both the encoder and decoder to enhance the modeling of spatial phase distributions, while the discriminator is designed to learn physically plausible beam distribution patterns and guide the generator toward producing more realistic outputs. As illustrated in Fig. 1, the overall model consists of three submodules: the Encoder, Decoder, and Discriminator. The model takes angular parameters (θ, ϕ) as input and outputs the phase values of 16 array elements, forming a 4×4 phase array image.

The encoder module takes as input a normalized phase distribution $x \in \mathbb{R}^{16}$, which is reshaped into a 4×4 2D image. Two convolutional layers are applied to extract spatial features: the first convolutional layer employs eight 3×3 kernels with a stride of 1 and padding of 1, while the second layer has the same structure but with 16 channels. The convolutional output is then flattened into a 256-dimensional feature vector, which is concatenated with the conditional information $c \in \mathbb{R}^2$, yielding a 258-dimensional input. A fully connected layer subsequently maps this vector to the mean $\boldsymbol{\mu}$ and log-variance $\log \boldsymbol{\sigma}^2$ of the latent space, from which the latent variable is sampled via the reparameterization trick:

$$\mathbf{z} = \boldsymbol{\mu} + \boldsymbol{\sigma} \odot \boldsymbol{\epsilon}, \quad \boldsymbol{\epsilon} \sim \mathcal{N}(\mathbf{0}, \mathbf{I}) \tag{6}$$

where $\boldsymbol{\sigma}$ is the standard deviation, $\boldsymbol{\epsilon}$ is a sample from the standard normal distribution, and $\odot$ denotes element-wise multiplication.

The decoder receives the concatenated latent variable $\mathbf{z}$ and conditional input, which are mapped to a 256-dimensional vector through two fully connected layers and then reshaped into a tensor of size $16 \times 4 \times 4$. Two deconvolutional layers are then applied to reconstruct the phase image: the first maps 16 input channels to 8 output channels, while the second reduces them to a single channel, producing a 4×4 phase image. ReLU activation functions are employed throughout the decoding process.

The discriminator aims to distinguish whether a predicted result corresponds to a physically valid phase distribution. It takes a 4×4 phase image as input, extracts spatial features through two convolutional layers, and flattens the output. The resulting vector is concatenated with the conditional information and passed through two fully connected layers to output a probability of authenticity. The final layer employs a Sigmoid activation function to produce a confidence score.

Through this design, the CVAE component ensures a consistent and valid mapping between outputs and the input angular conditions, while the GAN framework enhances the realism and physical consistency of the generated results. During training, the loss function integrates reconstruction error, Kullback–Leibler (KL) divergence, and adversarial loss to jointly ensure phase prediction accuracy and distribution plausibility.

Network training

To effectively train the proposed CVAE-GAN, a two-stage training strategy combining supervised pre-training and adversarial fine-tuning is adopted. In the pre-training stage, the discriminator is fixed while only the generator (encoder and decoder) is trained, with the objective of minimizing the reconstruction loss and KL

Downloaded from https://www.cambridge.org/core. UNIVERSIDAD AUTONOMA METROPOLITANA, on 11 Nov 2026 at 21:43:48, subject to the Cambridge Core terms of use, available at https://www.cambridge.org/core/terms. https://doi.org/10.1017/S1759078726103882

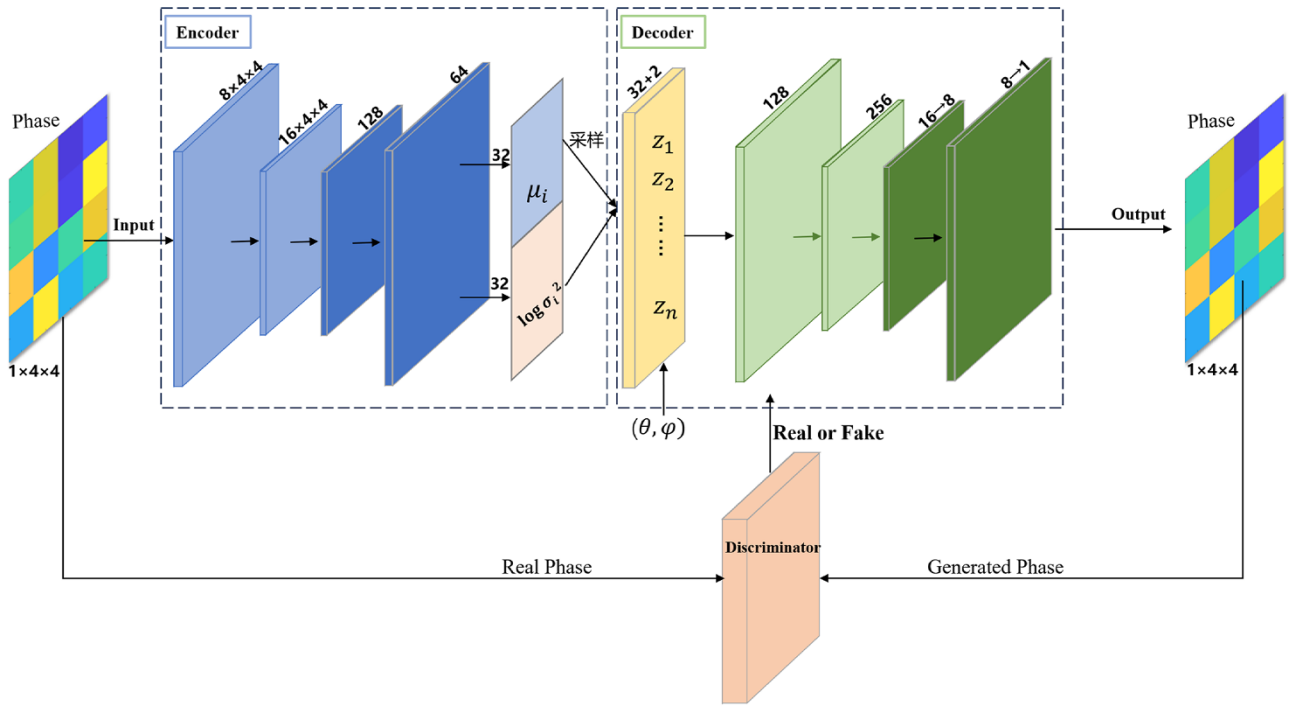


Figure 1. Schematic diagram of the CVAE-GAN model.

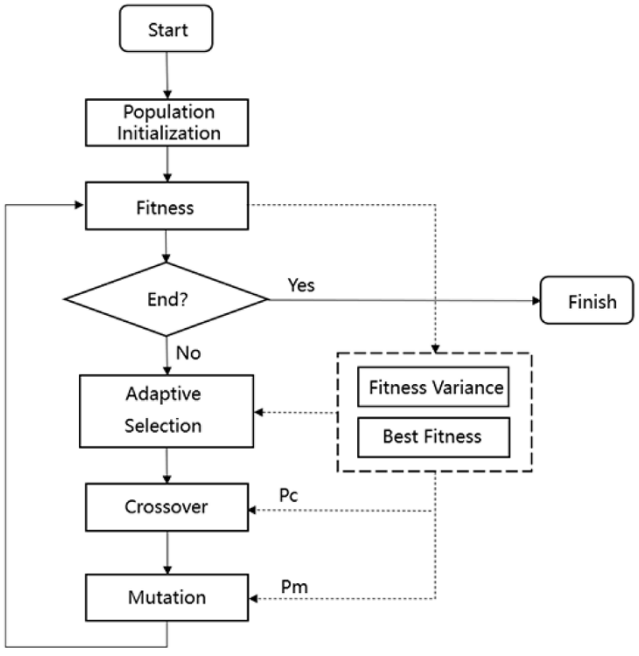


Figure 2. Schematic diagram of the improved genetic algorithm (IGA).

divergence. The loss functions are defined as:

$$L_{\mathrm{KL}} = \frac{1}{2}\sum_{i=1}^{d}\left(\mu_i^2 + \sigma_i^2 - \log\sigma_i^2 - 1\right) \tag{7}$$

$$L_{\mathrm{rec}} = \mathbb{E}_{x,z}\left[\|\hat{x} - x\|^2\right] \tag{8}$$

where μ_i and σ_i denote the mean and standard deviation output by the encoder, x is the ground-truth sample, and $\hat{x}$ is the reconstructed output given the conditional input c and latent variable $\mathbf{z}$. After pre-training, adversarial training is introduced. In this stage, the generator and discriminator are optimized in a minimax game, with their respective loss functions defined as:

$$L_D = -\mathbb{E}_x\left[\log D(x,c)\right] - \mathbb{E}_{\hat{x}}\left[\log\left(1 - D(\hat{x},c)\right)\right] \tag{9}$$

$$L_{\mathrm{GAN}} = -\mathbb{E}_{\hat{x}}\left[\log D(\hat{x},c)\right] \tag{10}$$

The total loss function of the CVAE-GAN is expressed as a weighted combination of all sub-losses:

$$L_{\text{CVAE-GAN}} = L_{\mathrm{KL}} + \beta L_{\mathrm{rec}} + \gamma L_{\mathrm{GAN}} \tag{11}$$

where β and γ are tunable hyperparameters that balance the contributions of different objectives. An alternating training strategy is employed, in which the generator is fixed while training the discriminator and vice versa, thereby ensuring that generated samples gradually align with the distribution of real data.

Results and analysis

Data generation

To support the training and evaluation of the beamforming model, a high-quality phase dataset was constructed based on an IGA to achieve desired radiation pattern characteristics, including main-lobe alignment and sidelobe suppression, as illustrated in Fig. 2. During each generation of evolution, the standard deviation of the population's fitness is calculated to quantify population diversity, and the improvement of the historical best fitness is used to assess whether the algorithm has stagnated. When the fitness variance is small, a roulette wheel selection strategy is employed to enhance the participation of individuals in evolution; when fitness differences are large, a tournament selection strategy is used

Downloaded from https://www.cambridge.org/core. UNIVERSIDAD AUTONOMA METROPOLITANA, on 11 Nov 2026 at 21:43:48, subject to the Cambridge Core terms of use, available at https://www.cambridge.org/core/terms. https://doi.org/10.1017/S1759078726103882

Table 1. Complexity and inference time comparison of different models

Algorithm	Parameters	Training time (100 epochs)	Inference time (per sample)
CVAE-GAN	15,000	4.6 min (2.76 s/epoch)	16 ms
MLP	9,680	0.8 min (0.48 s/epoch)	7 ms
RBF Network	2,448	0.5 min (0.3 s/epoch)	8 ms
GA (traditional)	–	–	8–10 s

to accelerate the inheritance of elite individuals. In cases where the algorithm stagnates or the evolution slows down, a rank-based selection strategy is applied to introduce more medium- and low-fitness individuals, thereby enhancing global search capability. The crossover probability P_c and mutation probability P_m are dynamically adjusted to decrease linearly over iterations. Higher probabilities are set in the early stages to strengthen global exploration, while lower probabilities are applied in later stages to improve local search accuracy.

Based on the aforementioned algorithm, the dataset was generated such that each sample consists of the desired main-lobe direction of the radiation pattern and the corresponding target phase distribution for a given angular pair (θ, φ). The construction procedure is as follows:

(1) **Angular range:** The elevation angle is defined as $\theta \in [-45^\circ, 45^\circ]$ and the azimuth angle as $\varphi \in [0^\circ, 180^\circ]$, sampled at 1° intervals.
(2) **Sample generation:** For each (θ, φ) pair, the GA is employed to obtain a phase distribution that satisfies the radiation pattern specifications. Each sample is represented as

$$\{\, c = [\theta, \varphi],\ x = [\phi_1, \phi_2, \ldots, \phi_{16}] \,\}$$

where c denotes the conditional angular input and x represents the 16-dimensional phase vector normalized to $[-1, 1]$.
(3) **Dataset size and split:** A total of 91 sampling points are selected for the elevation angle θ and 181 sampling points for the azimuth angle φ, resulting in $91 \times 181 = 16{,}471$ samples. The dataset is divided into 80% for training (13,176 samples) and 20% for testing (3,295 samples), with stratified random sampling applied to ensure a uniform distribution across all angles.

Simulation and testing

To demonstrate the effectiveness of the proposed method, all experiments were conducted on a unified hardware platform: an Intel Core i9-13980HX CPU, an NVIDIA GeForce RTX 4060 GPU (8 GB), and the Windows 11 operating system. The software environment consisted of Python 3.8, PyTorch 1.10, CUDA 11.3, and scikit-learn.

As shown in Table 1, the proposed CVAE-GAN model consists of an encoder (6,880 parameters), a decoder (4,848 parameters), and a discriminator (3,329 parameters), resulting in approximately 15,000 trainable parameters in total. For comparison, we also evaluated an MLP with 9,680 parameters and a radial basis function (RBF) network with 2,448 parameters under the same conditions.

Training the CVAE-GAN for 100 epochs took approximately 5 minutes, representing a one-time offline cost. After training,

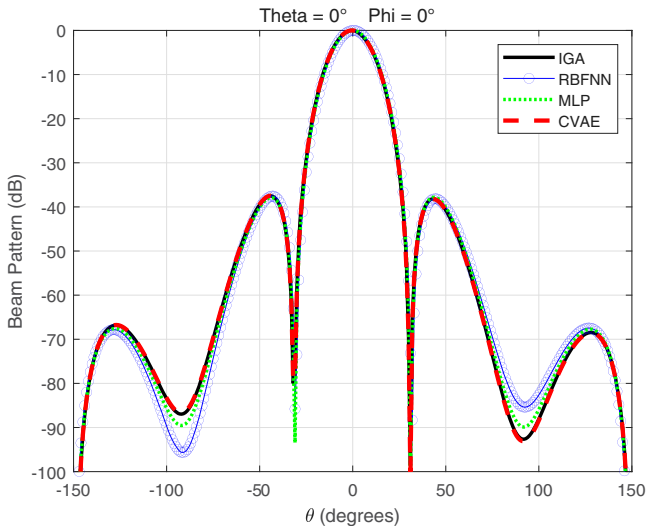


Figure 3. Far-field radiation patterns of the 4×4 planar array at the training-set angle $(0, 0)$ predicted by CVAE-GAN, RBFNN, MLP, and IGA.

inference on a single input pair (θ, ϕ) was performed on the GPU. As shown in Table 1 (averaged over 30 independent runs), the inference times are 16 ms for the CVAE-GAN, 8 ms for the RBF network, and 7 ms for the MLP. These inference times include data normalization and inverse transformation, reflecting the end-to-end prediction latency.

To validate the effectiveness of the proposed CVAE-GAN-based phase prediction model in practical beamforming tasks, tests were conducted under multiple specified incident angles, including both angles present in the training set and previously unseen angles. The phase vectors predicted by CVAE-GAN, RBFNN, MLP, and IGA-based predictions from the training set were respectively applied to a 4×4 planar array. By comparing the resulting radiation patterns, the beamforming accuracy and reliability of each method were evaluated in terms of main-lobe direction, amplitude distribution, and null positions.

Figure 3 illustrates the far-field radiation patterns of the 4×4 planar array loaded with phase vectors predicted by CVAE-GAN, RBFNN, MLP, and IGA from the training set at the training-set angle $(\theta, \phi) = (0, 0)$. It can be observed that the main-lobe positions of all methods accurately match the expected signal direction. However, in terms of sidelobe structures and overall radiation shape, the radiation pattern predicted by CVAE-GAN is the closest to that generated by IGA in the training set, with both the positions and amplitudes of sidelobes highly consistent. In contrast, RBFNN and MLP+GA exhibit noticeable deviations or leakage in the sidelobe regions. These observations indicate that CVAE-GAN demonstrates superior phase prediction accuracy and an outstanding ability to reproduce features present in the training set.

Figure 4 presents the full-angle amplitude error comparison between the predicted radiation patterns of different methods and the reference pattern at the training-set angle $(\theta, \phi) = (0, 0)$. It can be seen that CVAE-GAN exhibits the lowest overall error across the entire angular range, particularly maintaining small amplitude deviations in both the main-lobe and sidelobe regions, with the error curve closely following that of the IGA-generated training-set pattern. In contrast, RBFNN and MLP+GA show noticeable fluctuations in the sidelobe regions, indicating insufficient capability to approximate the true radiation pattern. These results further

Downloaded from https://www.cambridge.org/core. UNIVERSIDAD AUTONOMA METROPOLITANA, on 11 Nov 2026 at 21:43:48, subject to the Cambridge Core terms of use, available at https://www.cambridge.org/core/terms. https://doi.org/10.1017/S1759078726103882

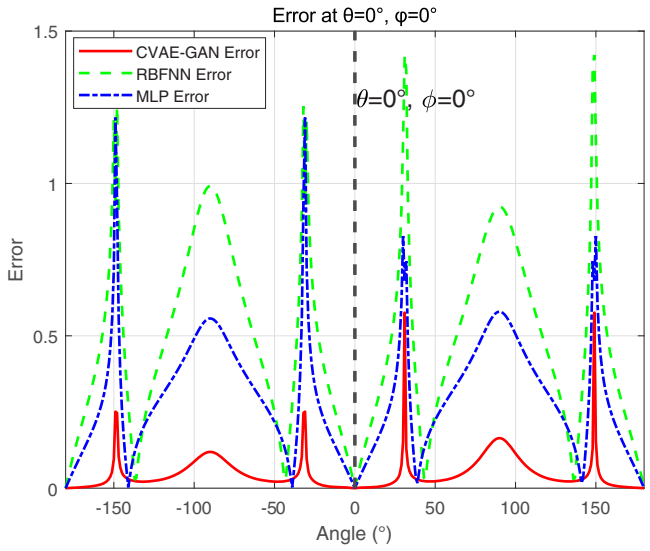


Figure 4. Full-angle amplitude error curves between predicted radiation patterns and reference pattern at $(0, 0)$.

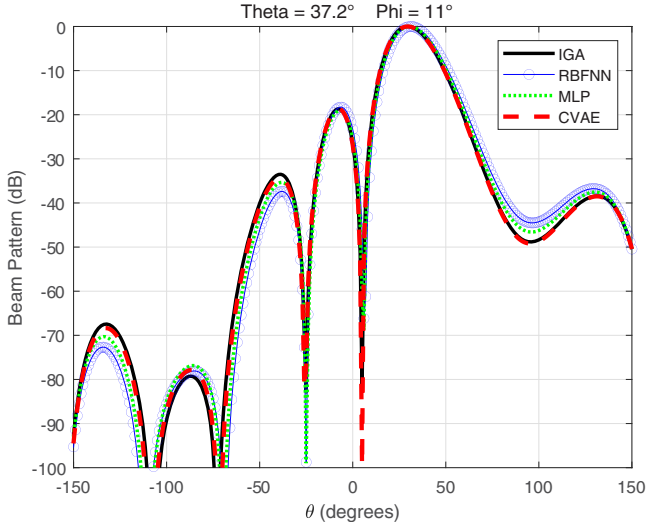


Figure 5. Far-field radiation patterns of the 4×4 planar array at the unseen angle $(37.2°, 11°)$ predicted by CVAE-GAN, RBFNN, MLP, and IGA.

confirm that CVAE-GAN not only accurately predicts the main-lobe direction but also effectively captures the amplitude features present in the training set, demonstrating superior performance in sidelobe control and overall beam pattern consistency.

Figure 5 illustrates the far-field radiation patterns obtained by loading the phase vectors predicted by different methods into a 4×4 planar array at an angle $(\theta, \phi) = (37.2°, 11°)$ not included in the training set. All methods maintain correct main-lobe steering; however, discrepancies appear in the sidelobe structure and overall radiation shape. The radiation pattern generated by CVAE-GAN is closest to the IGA-generated training-set pattern, with the first sidelobe nearly overlapping the reference pattern, whereas RBFNN and MLP exhibit noticeable amplitude inconsistencies in the sidelobe regions. These results indicate that CVAE-GAN can effectively preserve pattern consistency and stability even for angles unseen during training.

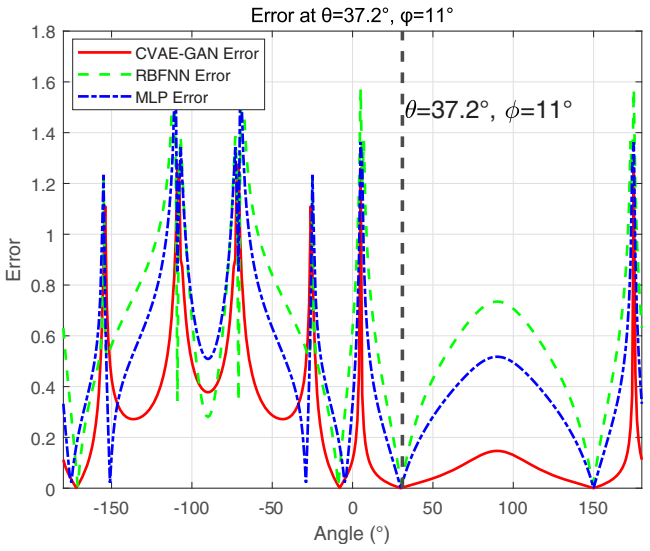


Figure 6. Full-angle amplitude error curves between predicted radiation patterns and reference pattern at $(37.2°, 11°)$.

Figure 6 presents the full-angle amplitude error curves under the same angular condition, providing a quantitative verification of the observations described above. It can be seen that CVAE-GAN exhibits significantly lower errors in both the main-lobe and first sidelobe regions compared with RBFNN and MLP and maintains a relatively low error level across the entire angular range, indicating more accurate predictions in key radiation directions. In contrast, RBFNN and MLP show noticeably larger errors in the sidelobe regions, reflecting their limited capability to capture the array's radiation characteristics. Overall, CVAE-GAN demonstrates superior generalization ability and enhanced sidelobe control for unseen angles.

Table 2 summarizes the mean squared error (MSE) of predicted radiation patterns for different methods under various steering angle conditions. It can be observed that CVAE-GAN consistently achieves significantly lower errors than RBFNN and MLP across all angles, demonstrating more stable and reliable performance. For angles present in the training set, e.g., $(\theta, \phi) = (0°, 0°)$, the MSE of CVAE-GAN is only 0.2690, which is far lower than RBFNN's 4.7146 and also substantially lower than MLP's 1.9557, indicating that the model can accurately reproduce the beam characteristics from the training set. Under unseen angles not included in the training data, CVAE-GAN also exhibits strong generalization capability; for instance, at $(\theta, \phi) = (37.2°, 11°)$, the error remains controlled at 2.9165, outperforming RBFNN (7.9823) and MLP (6.0117). Similar trends are observed for other test angles, showing that CVAE-GAN maintains a more balanced error distribution across different directions, particularly suppressing errors in the sidelobe regions and producing radiation patterns closer to reference results. These findings indicate that CVAE-GAN not only achieves high prediction accuracy for angles within the training set but also preserves stable performance for unseen angles, demonstrating superior precision, generalization, and robustness in beamforming tasks.

The proposed CVAE-GAN model consists of an encoder (6,880 parameters), a decoder (4,848 parameters), and a discriminator (3,329 parameters), totaling approximately 15,000 trainable parameters. For comparison, we also evaluated an MLP with 9,680 parameters and an RBF network with 2,448 parameters under

Downloaded from https://www.cambridge.org/core. UNIVERSIDAD AUTONOMA METROPOLITANA, on 11 Nov 2026 at 21:43:48, subject to the Cambridge Core terms of use, available at https://www.cambridge.org/core/terms. https://doi.org/10.1017/S1759078726103882

Table 2. MSE comparison of radiation pattern predictions by different methods

Algorithm	$\theta = 0^\circ$, $\phi = 0^\circ$	$\theta = 10^\circ$, $\phi = 3^\circ$	$\theta = 23.7^\circ$, $\phi = 25^\circ$	$\theta = 37.2^\circ$, $\phi = 11^\circ$
CVAE-GAN	0.2690	1.2227	2.2024	2.9165
RBFNN	4.7146	6.4194	6.7023	7.9823
MLP	1.9557	6.6477	1.3604	6.0117

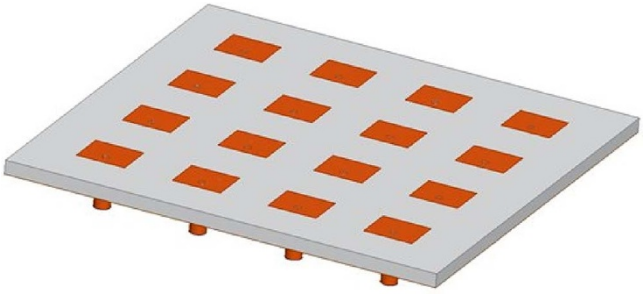


Figure 7. HFSS simulation model of the antenna.

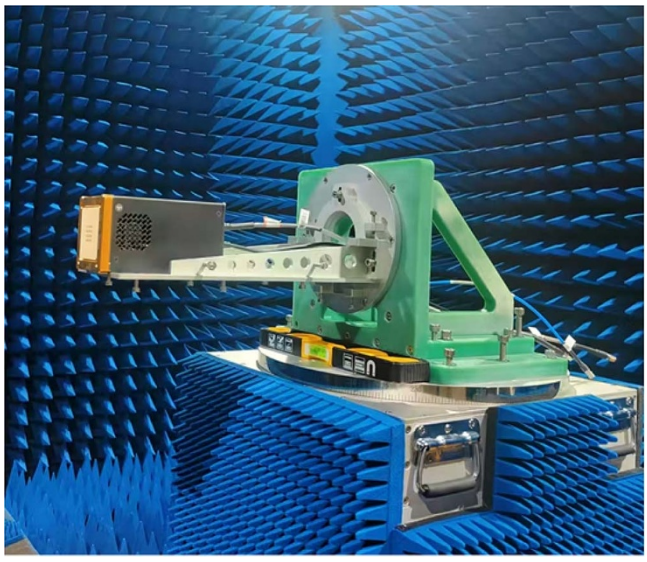


Figure 8. Phased array antenna testing setup in a microwave anechoic chamber.

identical conditions. Training the CVAE-GAN for 100 epochs required about 5 minutes, a one-time offline cost, while inference on a single input pair (θ, ϕ) on the GPU averaged 16 ms for the CVAE-GAN, 8 ms for the RBF network, and 7 ms for the MLP (over 30 runs, including normalization and inverse transformation). In contrast, traditional iterative methods such as GAs and particle swarm optimization (PSO) typically take seconds to minutes to synthesize a single pattern for a given (θ, ϕ). Although the CVAE-GAN inference time is slightly longer than that of the RBF network and MLP, it achieves significantly higher generation accuracy, especially in complex beamforming tasks requiring precise phase distributions. More importantly, compared with GA and PSO, the CVAE-GAN reduces online computational cost by two to three orders of magnitude (from seconds to milliseconds), fully meeting real-time beamforming demands. Its compact parameter count also makes it lightweight and suitable for edge deployment. In summary, the proposed CVAE-GAN effectively learns beam structure characteristics under varying incident angles, demonstrating superior accuracy and generalization over classical neural networks, thereby validating its practicality and reliability for complex beamforming prediction tasks.

To further assess the practical effectiveness of the CVAE-GAN model in phase prediction, the predicted phase distributions were applied to full-wave simulations and experimental tests of a phased array, using the resulting beamforming performance as an evaluation criterion. The phase vectors predicted by the CVAE-GAN were used as excitations for a 4×4 planar array. The array was modeled in High Frequency Structure Simulator (HFSS) 15.0 for electromagnetic simulation. The array configuration is shown in Fig. 7, with an operating frequency of 27 GHz, element spacing of half-wavelength ($\lambda/2$), and structural parameters consistent with those used during model training.

In addition, the same predicted phase vectors were applied to a physical phased array through a phased array driving platform. Figure 8 shows the far-field testing system constructed for the 4×4 array, which includes the antenna array, a phase control module, a vector network analyzer (VNA), and a precision rotation stage. During testing, the CVAE-GAN-generated phases were loaded onto the array, and the planar near-field radiation data at

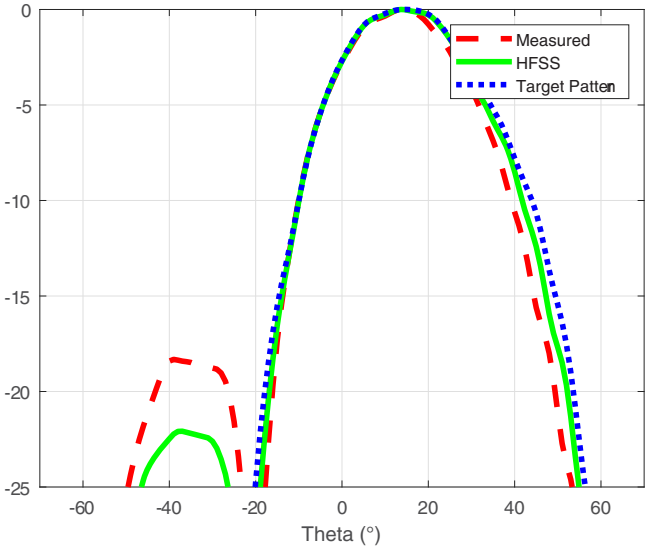


Figure 9. Measured and full-wave simulated radiation patterns.

different angles were collected using the VNA, which were then further transformed into the array far-field radiation patterns.

Figure 9 illustrates the comparison between HFSS simulation, physical measurement, and the target radiation pattern at the specified angles $\theta = 15^\circ$ and $\phi = -17^\circ$. It can be observed that the main-lobe directions of both HFSS simulation and physical measurement closely align with the target pattern, indicating accurate prediction of the main-lobe steering. Regarding the sidelobe positions and amplitudes, the HFSS simulation is relatively close to the target pattern, while the measured sidelobe amplitudes are slightly higher, but the overall shape remains consistent. Both HFSS simulation and physical measurement match the target pattern well, validating the accuracy and reliability of the CVAE-GAN output phases in practical beamforming tasks.

Figure 10 presents the full-angle amplitude errors of HFSS simulation and physical measurement relative to the target radiation pattern at the specified angles $\theta = 15^\circ$ and $\phi = -17^\circ$. It can be

Downloaded from https://www.cambridge.org/core. UNIVERSIDAD AUTONOMA METROPOLITANA, on 11 Nov 2026 at 21:43:48, subject to the Cambridge Core terms of use, available at https://www.cambridge.org/core/terms. https://doi.org/10.1017/S1759078726103882

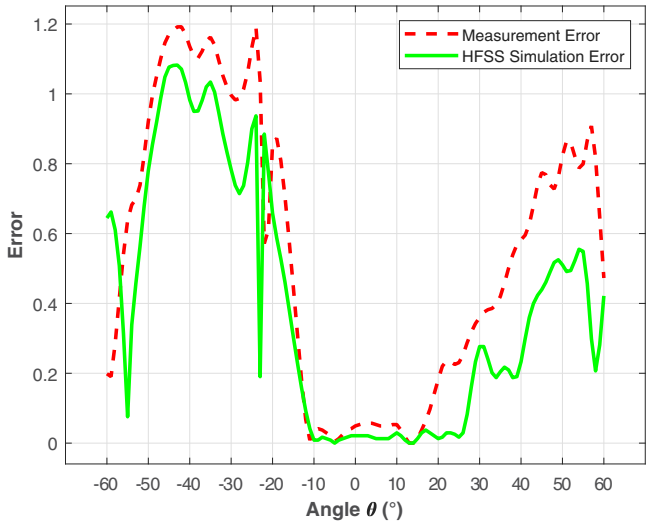


Figure 10. Full-angle amplitude error of HFSS and measurement.

seen that the error of the HFSS simulation in the main-lobe region remains below 0.2, indicating its ability to accurately reproduce the radiation characteristics of the target pattern. The measurement error is slightly higher than that of the simulation, but the overall trend closely follows the simulation results, demonstrating that the antenna radiation pattern generated using CVAE-GAN output phases aligns well with the expected pattern in both main-lobe and sidelobe regions. These results further confirm that CVAE-GAN output phases can achieve high-precision beamforming in practical array applications and indicate that both HFSS simulation and physical measurements exhibit reliable reproducibility.

The experimental results indicate that, both in simulation and physical testing, the radiation patterns generated by the CVAE-GAN exhibit high prediction accuracy. The root-mean-square errors of the full-wave simulations and physical measurements are 6.2 dB and 4.1 dB, respectively. The radiation patterns produced from the predicted phases closely match the target patterns, with accurate main-lobe directions, consistent sidelobe structures, and smoothly distributed overall errors.

Discussion on scalability and applicability to complex scenarios

While the proposed method is validated on a 4 × 4 planar array with phase-only steering as a proof-of-concept benchmark, the practical necessity of adopting a CVAE-GAN architecture becomes increasingly evident when considering more challenging deployment scenarios.

First, in terms of *scalability to larger arrays*, conventional iterative optimizers – such as GAs and sequential quadratic programming – exhibit a polynomial or even exponential growth in computational cost as the number of antenna elements increases. For an 8 × 8 or 16 × 16 UPA, the dimensionality of the solution space expands dramatically, making real-time beamforming extremely difficult with traditional methods. In contrast, our encoder–decoder backbone relies primarily on the channel dimensions of the convolutional layers; the forward inference time scales roughly linearly with the array size, as the computational bottleneck lies in the convolution operations rather than the number of array elements. This property makes the proposed framework particularly attractive for large-scale arrays where real-time performance is critical.

Second, regarding *generalization to more complex beamforming constraints*, our architecture is not inherently limited to phase-only control. By simply expanding the output dimensionality of the decoder, the network can directly generate both amplitude and phase excitations (i.e., complex-valued weights), accommodating scenarios that require dynamic range ratio constraints or simultaneous sidelobe suppression. Furthermore, for advanced tasks such as multi-beam forming or precise null steering with multiple interference directions, the optimization landscape becomes severely ill-posed and multi-modal – i.e., multiple distinct excitation distributions can yield similar radiation patterns. The conditional latent space of the CVAE is specifically designed to encapsulate such one-to-many mappings via its stochastic sampling mechanism, a capability that purely deterministic networks (e.g., MLP or standard CNN) or analytical methods inherently lack.

Therefore, while the current 4 × 4 phase-only configuration serves as a rigorous feasibility demonstration, the core strengths of the CVAE-GAN – scalable real-time inference, adaptability to complex-valued outputs, and multi-modal solution representation – are expected to play a pivotal role in future large-scale and complex-constrained beamforming systems.

Conclusion

This paper proposes a CVAE-GAN-based beamforming method that demonstrates significant advantages in prediction accuracy and practical applicability. By constructing a high-fidelity training dataset using an IGA, the beamforming problem is effectively transformed into a phase matrix prediction task. On this basis, the designed CVAE-GAN network integrates conditional generation and adversarial learning mechanisms, enabling the predicted array phase distributions to produce accurate beamforming in both HFSS full-wave simulations and physical experiments. The results validate the physical feasibility and accuracy of the proposed method in real antenna systems. Future work will focus on extending the proposed framework to larger array configurations (e.g., 8 × 8 and 16 × 16), incorporating amplitude-phase joint optimization, and validating its performance under more stringent constraints such as multi-null steering and sidelobe envelope control.

Funding statement. This work was supported by the Leading Innovative and Entrepreneurial Team Program of Zhejiang (Grant No. 2023R01003).

Competing interests. The authors declare no competing interests.

References

1. **Tauqir HP and Habib A** (2019) Deep learning based beam allocation in switched-beam multiuser massive MIMO systems. In *Proceedings of the 2nd International Conference on Latest Trends in Electrical Engineering and Computer Technology (INTELLECT)*. 1–5.
2. **Kassir HA, Zaharis ZD, Lazaridis PI, Kantartzis NV, Yioultsis TV and Xenos TD** (2022) A review of the state of the art and future challenges of deep learning-based beamforming. *IEEE Access* **10**, 80869–80882.
3. **Xu Y, Zhu H and Guo YJ** (2024) Compact multi-beamforming networks based on generalized joined coupler matrix with flexible beam angles and low sidelobe levels. *IEEE Open Journal of Antennas and Propagation* **5**(4), 810–822.
4. **Zhang X, He Z, Liao B, Zhang X and Peng W** (2017) Pattern synthesis with multipoint accurate array response control. *IEEE Transactions on Antennas and Propagation* **65**(8), 4075–4088.

Downloaded from https://www.cambridge.org/core. UNIVERSIDAD AUTONOMA METROPOLITANA, on 11 Nov 2026 at 21:43:48, subject to the Cambridge Core terms of use, available at https://www.cambridge.org/core/terms. https://doi.org/10.1017/S1759078726103882

5. **Bahingayi EE and Kyungchun L** (2022) Low-complexity beamforming algorithms for IRS-aided single-user massive MIMO mm-wave systems. *IEEE Transactions on Wireless Communications* **21**, 9200–9211.
6. **Liu Z, Zhao X, Zhang Y Chen X** (2024) Pattern synthesis method of antenna array based on iterative adaptive convex optimization, Journal of Microwaves. 27 February 2024.
7. **Feng L, Zhang J, Chen K, Wang Y and Li H** (2020) Phased array beamforming with practical constraints. *Signal Process* **176**, 107698. https://doi.org/10.1016/j.sigpro.2020.107698.
8. **Boeringer D and Werner D** (2002) Adaptive mutation parameter toggling genetic algorithm for phase-only array synthesis. *Electronics Letters* **38**(25), 1.
9. **Mu ZQ** (2023) Research on array antenna beamforming technology based on intelligent algorithm, PhD thesis. Beijing University of Posts and Telecommunications.
10. **Cui C, Li WT, Ye XT, Rocca P, Hei YQ and Shi XW** (2021) An effective artificial neural network-based method for linear array beampattern synthesis. *IEEE Transactions on Antennas and Propagation* **69**(10), 6431–6443.
11. **Zhang Y** (2025) Research on real-time array beamforming method based on deep learning, PhD thesis. University of Electronic Science and Technology of China.
12. **Zhang B, Lu M, Chen Z and Cao Y** (2015) Beamforming algorithm based on radial basis function neural network. *Journal of Xi'an University of Posts and Telecommunications* **20**(6), 55–59.
13. **Zhang S, Yuan D and Wang G** (2024) Intelligent surface millimeter-wave beamforming based on deep learning. *Radioengineering* **54**(7), 1732–1738.



Yuhao Zhang received the B.S. degree in Communication Engineering from Qingdao University, Qingdao, China, in 2023. He is currently pursuing the M.S. degree in Information and Communication Engineering at Hangzhou Dianzi University. He has participated in several projects related to antenna optimization and signal processing. His research interests include deep learning for array signal processing, adaptive beamforming, and antenna design.



Hongjun Chu was born in Henan, China, in 1987. He received the B.S. degree in electronics and information engineering from Harbin Engineering University in 2010, and the M.S. degree in electromagnetic field and microwave technology from Harbin Institute of Technology, Harbin, China, in 2015, where he is pursuing the Ph.D. degree in information and communication engineering. His research interests include metamaterials, millimeter-wave imaging, and radar.



Wenzhi Li received his Ph.D. degree in Information and Communication Engineering from Harbin Institute of Technology. He has published six papers in top journals including Nature Communications, IEEE IoTJ, and IEEE TMTT. He is currently a Distinguished Researcher at the Institute of Space Information, Hangzhou Dianzi University. His research interests include metasurfaces, computational imaging, and wireless power transfer.



Zhaohui Song is a professor and Ph.D. supervisor. He received his B.S., M.S., and Ph.D. degrees in Electronic Engineering, Electromagnetic Field and Microwave Technology, and Signal and Information Processing from Harbin Institute of Technology. From 1992 to 2012, he was a professor at Harbin Institute of Technology. He is currently the director of the Space Information Research Institute, Hangzhou Dianzi University.



Xingyu Zhou received the B.S. degree from Changshu Institute of Technology in 2024 and is currently pursuing his M.S. degree at Hangzhou Dianzi University. His research interests include array signal processing and applications, phased array beamforming algorithms, and deep learning.

Downloaded from https://www.cambridge.org/core. UNIVERSIDAD AUTONOMA METROPOLITANA, on 11 Nov 2026 at 21:43:48, subject to the Cambridge Core terms of use, available at https://www.cambridge.org/core/terms. https://doi.org/10.1017/S1759078726103882